Impact propagation effects along reinforced concrete beam

Downloaded from: https://research.chalmers.se, 2024-04-25 01:36 UTC

Citation for the original published paper (version of record):
Zanuy, C., Sanz, G., Johansson, M. et al (2019). Impact propagation effects along reinforced concrete beam. IABSE Symposium

N.B. When citing this work, cite the original published paper.

research.chalmers.se offers the possibility of retrieving research publications produced at Chalmers University of Technology.
It covers all kind of research output: articles, dissertations, conference papers, reports etc. since 2004.
research.chalmers.se is administrated and maintained by Chalmers Library

(article starts on next page)

IABSE Symposium 2019 Guimarães
Towards a Resilient Built Environment - Risk and Asset Management
March 27-29, 2019, Guimarães, Portugal

Impact propagation effects along reinforced concrete beams

Gonzalo S.D. de Ulzurrun*, Carlos Zanuy

Dept. Continuum Mechanics & Structures, Universidad Politécnica de Madrid, Spain

Morgan Johansson, Rasmus Rempling

Dept. Civil & Environmental Eng., Chalmers University of Technology, Gothenburg, Sweden

Contacting author: g.ulzurrun@caminos.upm.es (orcid.org/0000-0002-6733-1555)

Abstract

This paper studies the time-dependent structural behaviour of concrete beams subjected to impact loading. Drop-weight tests have been carried out in 1180 x 100 x 100 mm longitudinally reinforced concrete beams. Experimental results have been obtained by combing a high speed camera with two-dimensional digital image correlation. The analysis focused on the dynamic internal forces distribution and wave propagation. Flexural moments and, especially, shear forces were greater than their static strengths, confirming the strain-rate dependence of both failure mechanisms and clarifying the sensitivity of concrete to develop brittle failure. Wave propagation analysis showed a variable velocity, decreasing as the slenderness of the effective span increased.

Keywords: impact; internal forces; wave propagation; beams; concrete; digital image correlation.

1. Introduction

Lately, there is a growing public consciousness of need to guarantee structural concrete performance against high-speed loads due to, among others, natural hazards or terrorist attacks. Amid those extreme loads, impacts of rigid bodies at moderate speeds may occur, producing severe damage to structures. Impact loads are characterized by their impulsive nature, with high peak load, considerable strain rates and large energy release.

Among the structures that may be subjected to impact loads, such as rockfall protection galleries, underpass piers and airport or industrial paving, concrete structures may be critical. Reinforced concrete (RC) is sensitive to develop a brittle failure by shear or punching when subjected to high loading rates [1, 2], with a limited capacity for deformation and energy absorption, even in members reinforced with stirrups [3]. Some codes [4, 5] have addressed brittle failure by limiting the reinforcement ratio of impact exposed structures to 0.5% and 1.1%, respectively. Ulzurrun et al. [6] have shown that concrete beams with higher reinforcement ratio may avoid brittle failure by using steel fiber-reinforced concrete (SFRC). However, there is no generally accepted shear strength design criterion for RC structures under impact conditions.

In order to evaluate shear or punching strength in RC structures subjected to impulsive loads, it is necessary to know in advance the time dependent distribution of internal forces during impact loading. This distribution differs from the quasi-static one due to development of inertia forces and wave propagation [3, 7–9]. Nevertheless, there is some disagreement between authors when

describing both phenomena. This is explained by the difficulty to register experimentally cinematic parameters at numerous points along a beam. In order to predict the distribution evolution of internal forces, further research needs to be done.

An interesting way to study beams behaviour under impact loads is by using full-field measurement methods. Digital image correlation (DIC) is a well extended, robust and easy to implement full-field non-contact measurement system [10]. This technique analyzes deformations of a surface covered with a speckle pattern through dividing the image in a set of subimages, known as facets. The displacement field is obtained by tracking grey scales within facets, comparing pictures of the reference stage, before loading, with the deformed beam. This technique has been used by some authors in combination with high speed photography (HSP) to study dynamic tests [11], showing interesting results.

In this paper three slender RC beams subjected to impact load are analysed using 2-D DIC. These beams are part of a broader experimental campaign carried out by Jönsson and Stenseke [12]. Impact tests were performed with a drop weight rig at the Laboratory of Structural Engineering at Chalmers University of Technology, Sweden. The results have been analysed in terms of internal forces distribution and wave propagation velocity along time. A study of these same tests has been done by Johansson et al. [13] in terms of measurement resolution and stability of the results, showing its sensitivity to facet properties. Their conclusions have been taken into account in the analysis done in the following sections.

2. Experimental research

2.1 Test description

The experimental campaign covers three identical prismatic RC beams. These were named numerically, from 12 to 14. The dimensions of the beams were 1180 mm length, with square cross-section of 100 mm side. A reinforcement ratio ρ = 0.7% was chosen, which consisted in four bars of 6 mm diameter, distributed in the top and bottom faces, providing a concrete cover of 17 mm from beam faces. No transversal reinforcement was incorporated. Tests were completed in a three-point bending configuration, with a span length of 1000 mm between supports. Hence, the shear span-to-effective depth ratio was a/d = 6.25. An overview of the beam set-up is shown in Figure 1.

The impact tests were performed with a drop weight testing rig, which dropped from 5 m of height a 20 kg free falling mass, reaching an impact velocity of 9.9 m/s. The mass consisted in a solid steel cylinder of 80 mm diameter and 500 mm height, that struck beam midspan top face with spherical surface of 200 mm radius. The beam was simply supported with two solid steel rolls of 80 mm diameter, that were not intended to prevented beam uplift upon impact loading.

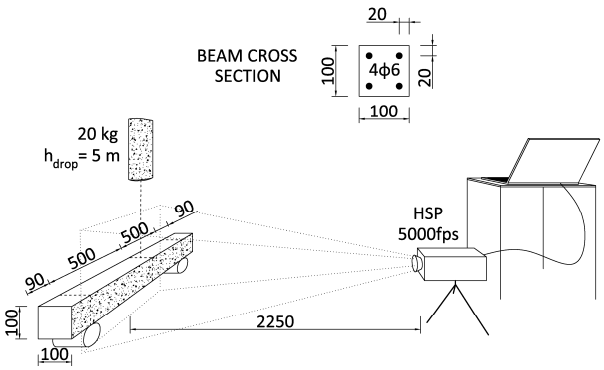

Figure 1. Schematic test set-up. Dimensions in mm.

A single HSP camera recorded the tests. Taking advantage of set-up symmetry only one half of the beam was framed, increasing image spatial resolution. The camera used was a Photron SA4 with a Tamron AF 28-75/2.8 lens. The camera body was placed perpendicular to the lateral surface of the beam at 2225 mm of distance, focal length was set to 75 mm and the aperture to f/2.8. The resolution of the recorded images was 1024 × 512 pixels, acquired at a ratio of 5 kHz, with a shutter speed of 1/5000 s. The spatial scale has been calibrated with a 60 mm gauge block, which indicated that the pixel size was 0.61162 mm. Thereby the field of view is 626.30 × 313.15 mm^2, covering the impact area at midspan as well as almost half beam length, leaving out of the frame 44 mm of the beam end, as it is shown schematically in Figure 1. In addition, measurement points are set-back from the boundaries about half of a facet size, increasing the length of the beam end not analysed to 54 mm.

Recorded images were analysed with 2-D DIC technique. A speckle pattern was applied on the beam and drop weight surface. The pattern consisted of black flecks, applied with a natural sea sponge over white background paint. Due to high recording speed an extra light source was employed during tests. The software used, GOM Correlate, builds discrete measurement points, which are tracked by square facets. Full-field measurements are obtained through a triangular mesh formed by facets that covers beam surface. According to the results presented by Johansson et al. [13] measurements are sensitive to facet properties, especially accelerations and strains that only showed consistent results with large facet sizes. In this study individual facets were employed to obtain measurements of the drop weight, while facet mesh provided full-field measurements at beam surface. Both employed a 32-pixel facet size, with a distance between mesh points of 12 pixels (size-to-distance ratio was 3/8). Measurement noise has been reduced by spatial average between equivalent points.

2.2 Material characterization

Concrete mix was prepared with ordinary Portland cement II. Water/cement ratio was 0.60, aggregates with a maximum size of 16 mm and GLENIUM 51/18 superplasticizer were used. The average compressive and tensile strength of concrete at the age of testing was 38 MPa and 4.8 MPa, respectively, with a fracture energy in the splitting tests of 0.14 kN/m. Reinforcing steel bars were of quality B500C according to Eurocode 2 [14], with a characteristic yield strength of 500 MPa. For further description of materials refer to [12].

2.3 Experimental results

All tested specimens exhibited a plastic response with a clear formation of a plastic hinge at midspan, which showed additional capacity in subsequent quasi-static tests done by Jönsson and Stenseke [12]. The hinge was delimited by shear plug cracks at both sides. These cracks did not progress through the compression side. Besides, thinner cracks developed between supports and midspan. Those cracks developed in the top face in a first stage. But, as impact load propagated, top cracks became imperceptible and the cracking progressed through the bottom face. This can be seen in the crack patterns presented in Figure 2, computed with the DIC system from principal strain diagrams.

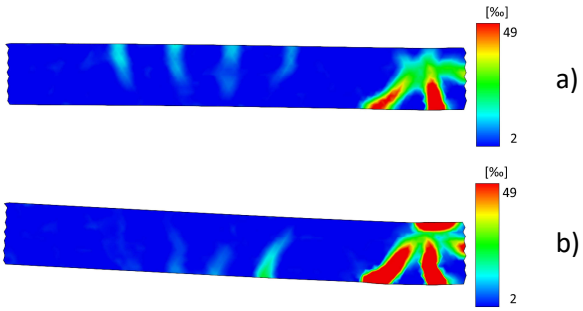

Figure 2. Beam 12, principal strain-rate diagrams: a) 1.4 ms and b) 4.6 ms after impact.

The mean deflection and acceleration evolution, in the first 6 ms after impact, along Beam 12 are shown in Figure 3, where the horizontal axis corresponds to the distance to support. Beam height was divided in four horizontal equal sections. Results were obtained as the average of the measurements at the middle line of each section. This avoids local effects and reduces noise levels. Measurements in all sections were rather similar, with limited noise scattering. However, at midspan, certain divergence was observed once diagonal plugging cracks developed, with larger deviations in the lower sections due to higher crack influence. No measurements of the last 54 mm at beam end were made. Instead, those were determined by extrapolation of the 20 mm next to facet mesh boundaries, being represented with dotted lines in the Figures presented.

Deflections, shown in Figure 3 a), did not reach a significant value, over the noise levels, until 0.6 ms after impact, showing large increases thereafter. The profile of the deflection showed a V-shape, with large curvatures concentrated in the plastic hinge at midspan. Uplift was visible at beam ends, occurring in the section over the support between 0.8 and 4.8 ms after impact loading. Accelerations, shown in Figure 3 b), also showed a V-shape until reaching its peak value 0.6 ms after impact beginning, exceeding 1500 g. Afterwards the profile became somewhat more even, with some oscillations between the central area and the edges. Similar results for both measurements were

observed in the other beams. However, moderately higher peak accelerations were registered in Beam 13.

Drop-weight acceleration was measured by spatial averaging four facet points distributed in the drop-weight side surface, close to the impact area. Impact force was directly obtained from this measurement and the drop-weight mass. Similarly, beam inertia forces distribution was obtained directly from the accelerations, shown in Figure 3 b), by considering RC density as 2500 kg/m^3. The resultant of inertia force for the whole beam was computed as the integral of beams inertia forces, including the extrapolated edges and taking symmetry in advantage. By applying the dynamic equation of motion to the acting forces, namely impact, inertia and sum of support reactions, the latter could be deduced, as it is presented in Figure 4 for Beam 12. In this Figure it can be seen that the impact force consisted of a high frequency peak followed by a smother peak, which was resisted by the inertia forces. Subsequently, resultant forces were zero with a slight increase just before the beam contacted the supports again. In that instant reaction forces developed, showing a large peak increase, rather smoother than the impact load. The lag between both loads, 4.8 ms, might be explained by a combination of wave propagation and local uplift.

Knowing impact, reactions and inertia loads, and their distribution, it is possible to obtain the internal forces diagrams along the beam. However, the reactions shown in Figure 4 present some spurious components while the beam was not in contact with the supports, during its uplift. These spurious reactions result of the addition of measurement noise and the cut-off high frequency components by the sampling rate employed. The resultant internal forces diagrams, shown in Figure 5, do not include these spurious reactions. These diagrams show the internal forces at different stages, until peak reaction is registered, 5 ms after impact. There were three different stages. Firstly, impact load and the inertia forces governed internal forces distribution, showing high and concentrated pointed peaks at midspan, which spread towards the supports with time. This is followed by a stage, characterized by smoother peaks, where inertia forces dominated, even though its resultant force was equal to zero. In this stage, shear peak force, which shifted its position between midspan and supports, was especially low. Subsequently, reactions developed producing high peak loads, localized at midspan and supports for bending moment and shear, respectively. In contrast with other stages, internal loads distribution in this stage resembles somehow to the static diagram of a uniformly loaded beam, probably to the even distribution of inertia forces.

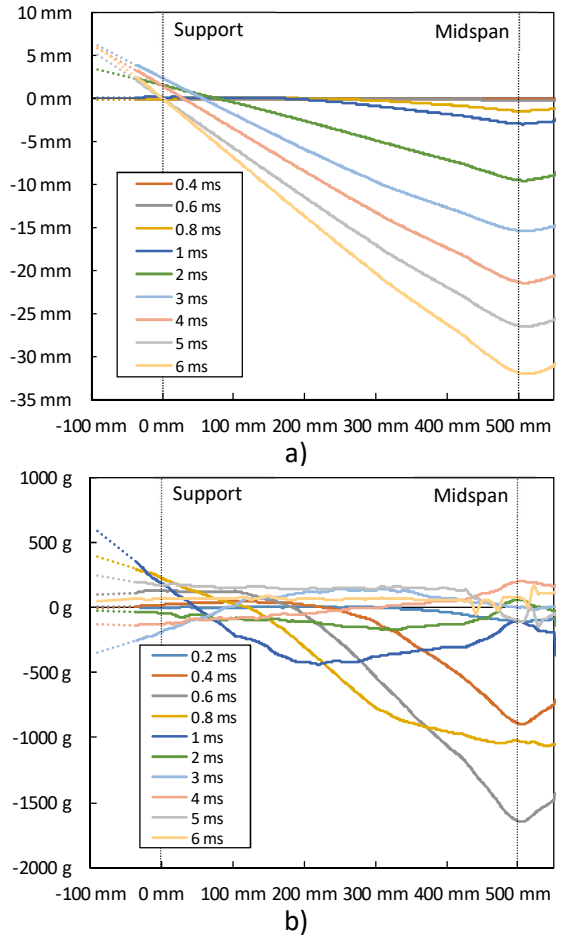

Figure 3. Measured parameters evolution for Beam 12: a) deflections; b) accelerations.

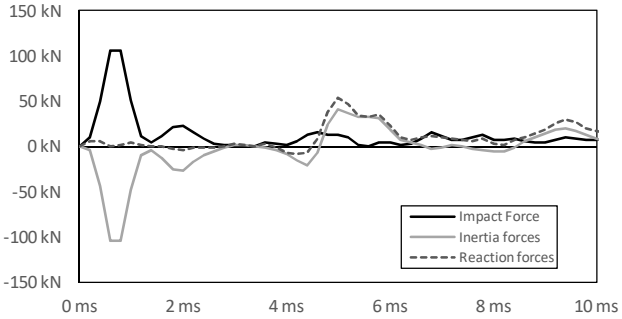

Figure 4. Acting forces on Beam 12 during impact.

Figure 5 b) shows that, in some stages, negative bending moments developed at beams ends. In the first instants, upward inertia forces grew so high that some countering downward inertia forces developed at beam ends, producing large negative flexural moments. Negative bending, would be the cause for beam top face cracking, as shown in Figure 2 a). By examining early impact stages, it is evident that the beam behaved similarly to a fixed beam with a variable length. This, has previously been described as the effective response length by Cotsovos et al. [8], and it will be referred to as effective span in this paper.

3. Analysis of results and discussion

3.1 Propagation of impact wave

It is clear from the results presented in the preceding section that beam response to impact loading did not affect its whole length at once. Results show how impact wave propagated along beam length, from midspan to supports. An interesting way to study this effect is by normalizing the deflection diagram. Figure 6 presents deflection distribution as the ratio to peak deflection for each stage, after subtracting support movement. Only the deflections diagrams visible over noise are presented. In the first stages deflection shape showed different curvatures with opposed sign, at midspan and at the edges of the effective span. As the impact wave propagated, that secondary curvature faded until its complete disappearance once the impact wave reached the supports.

Some authors [6, 7, 15] have measured the impact propagation time as the elapsed time between impact and initiation of support reaction. The corresponding average wave propagation velocities, in the range of 250 to 1250 m/s, were much lower than that of shear and axial waves in concrete structures. Besides, variable velocities registered indicate a dispersive behaviour for this wave. This can be confirmed by Figure 6, which clearly demonstrates that impact wave propagates from impact point to the supports at a variable rate, which decreases with time, as the effective span length increases. If the propagation velocity is computed for the presented tests based on the reaction lag, the resultant average propagation velocities, around 100 m/s, are much lower than those of [7] with equivalent geometry. This could be due to beam uplift observed over supports. In the studies mentioned above, beam uplift over

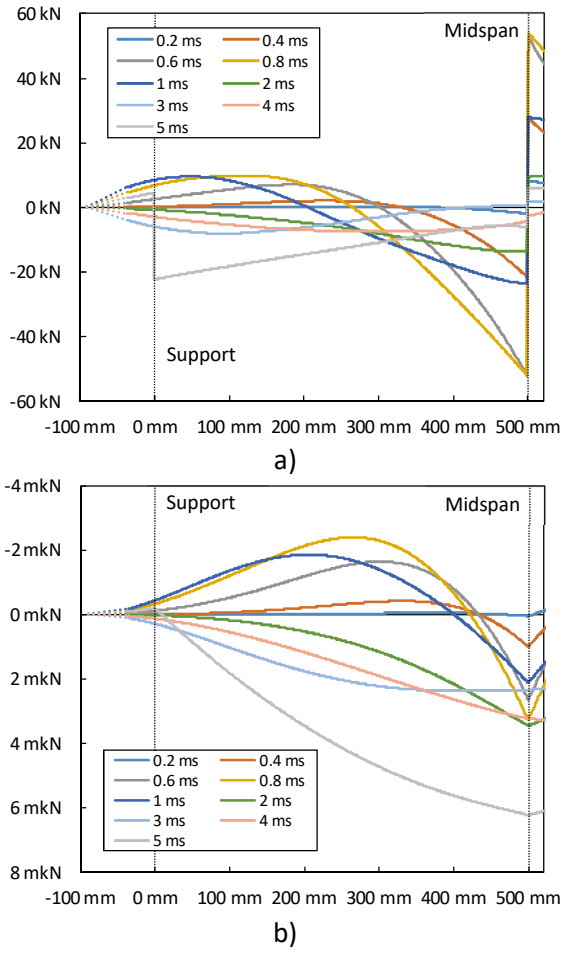

Figure 5. Internal forces distribution along Beam 12: a) shear forces; b) bending moment.

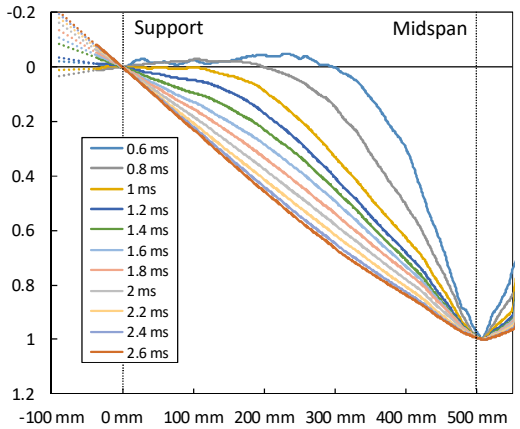

Figure 6. Beam 12 normalized deflection diagram.

supports was negligible according to their results or the set-up, including vertical constrains. In the presented tests, large uplift over support lags reactions, as the beam required additional time to strike the supports once the impact wave reached its whole span.

Figure 7 studies impact propagation by monitoring beam displacements over the support. If there was no beam uplift over the support, the reaction would have commenced once the beam started to descend towards the support. Therefore, it could be assumed that the propagation time is the time period since the beginning of impact until the vertical velocity of the beam over the support reaches zero; i.e., just before going downwards. By studying vertical velocities distribution over time, shown in Figure 8 as the ratio to peak vertical velocity, it is possible to define the effective span length at each time frame as the double of the distance from midspan to the point with vertical velocity equal to zero, taking advantage of symmetry.

An interesting way to validate this methodology is to compare the results with the similar tests from the literature. According to Isaac et al. [7] average propagation velocity is sensitive to beam slenderness. The results of that study, in addition to the findings of other studies [3, 6, 15], are presented together with the results of this paper in Figure 9. Presented results have been computed according to effective span length based on its vertical velocity distribution as function of time, whereas other authors results were computed with the reaction lag time, obtaining only one result per test. The comparison shows how literature results are in agreement with the findings of the present paper. Average propagation velocity decreased as the effective span to depth ratio increased, showing a variable velocity during wave propagation. This could be explained by considering the impact propagation as a flexural wave, according to McGhie [16], which decreases its velocity with the reduction of stiffness, linked to the effective span increase. Some scattering is visible among presented studies, this could be explained by the different span to lateral overhang ratios. Tests of Saatci et al. [3] show high propagation velocities compared to the tests of Ulzurrun and Zanuy [6, 15], with a span to lateral overhang ratio of 3.2, 11.1 and between 8 to 10, respectively. This might also explain the reason why average propagation velocity of the presented tests decreased suddenly as the effective span approached to lateral overhangs. Other factors, such as reinforcement layout and failure mode could also cause some divergences in propagation velocity.

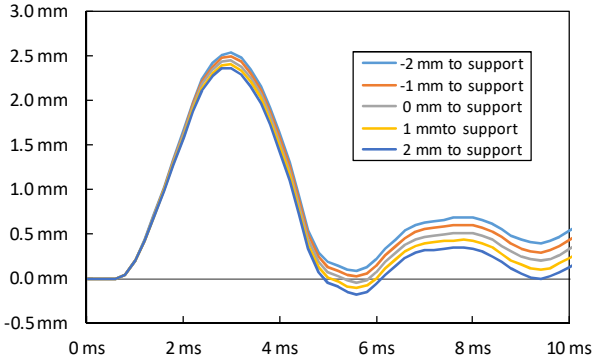

Figure 7. Vertical motion over time of Beam 12 points over support.

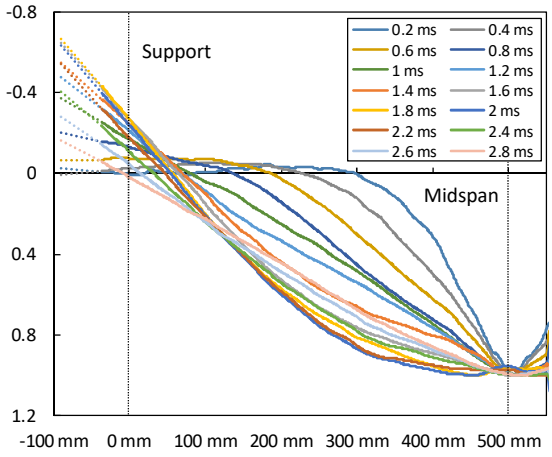

Figure 8. Beam 12 normalized vertical velocity diagram.

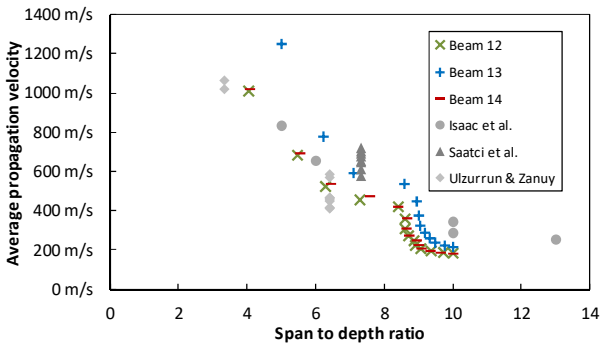

Figure 9. Comparison of average propagation velocity with results from literature [3, 6, 7, 15].

In addition, Figure 9 confirms that the methodology employed in this paper to track the effective span, could be employed to measure wave propagation regardless of support conditions. Other measurements, such as curvature or bending moment distribution, could be used as well to analyse effective span length. Nevertheless, those measurements include higher errors as both are obtained, directly or indirectly, by double numerical differentiation [13], being less reliable than velocity distribution.

3.2 Internal forces under impact loading

Shear and bending unfactored strength of tested beams, based in Eurocode 2 [14] formulations under static conditions, are 8.6 kN and 2.2 kNm, respectively. If these values are compared with peak internal forces in Figures 5 a) and b), 54.1 kN and 6.2 kNm, respectively, it confirms that the strength under dynamic conditions is higher than the static for both failure mechanisms. An interesting way to characterize this increase is through the dynamic increase factor (DIF) of the strength, a ratio between the dynamic and static strength, which results in 6.3 and 2.8 for shear and flexure, respectively. This indicates that shear failure mechanisms are more sensitive to loading rate under impact conditions. It should be noted that all beams presented diagonal cracks that did not develop completely, being flexure the governing failure mechanism. Therefore, shear DIF could have reached even higher values, before becoming the governing failure mechanism.

As it has been mentioned above, impact-loaded beams have shown high sensitivity to develop shear failure. Although the presented tests failed by flexure, the internal forces distribution, shown in Figure 5, might be an indicator of the causes of shear sensibility. Figure 10 shows the bending to shear force relationship at critical sections during impact. Those correspond to the sections where main cracks are located, namely at midspan and at the section located an effective depth form that. These diagrams show two differentiated stages, one that developed in firstly where shear is the dominating force, and a second stage that corresponds to the behaviour of the beam once impact load ceased to be the dominating force. In the latter, flexural forces govern beam behaviour.

Comparing impact behaviour with the static one it is visible that the effective shear span was lower than the corresponding to the set-up geometry. Hence, wave propagation and inertia forces distribution played an important role in the internal forces distribution evolution. Therefore it can be concluded that sensibility to brittle failure could be due to those factors.

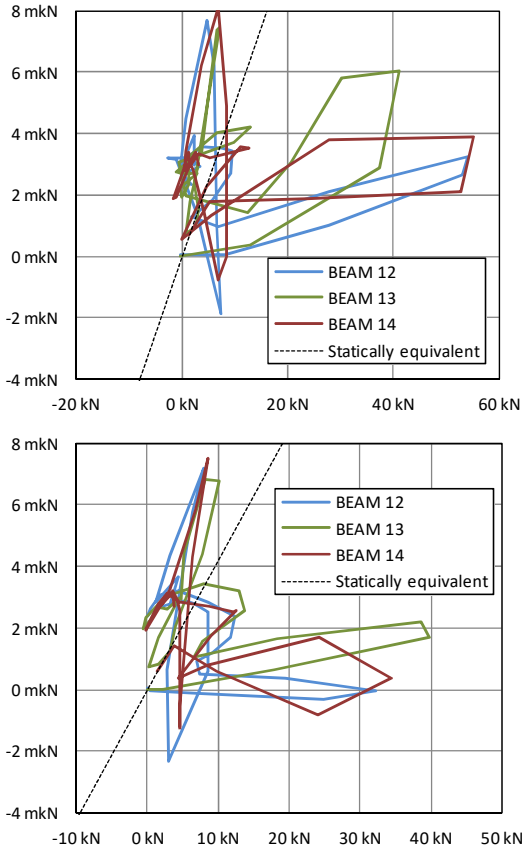

Figure 10. Flexure to shear relationship at sections: a) midspan; b) effective depth from midspan.

4. Conclusion

Experimental results of three impact tests carried out on RC beams are presented and discussed in this paper. The tests were recorded with a HSP camera and analyzed with 2-D DIC, a full field non-contact measurement system. Result analysis focused on the distribution of internal forces and impact wave propagation.

Impact load has shown to propagate along the beam at a variable rate, as flexural wave, which has a dispersive nature. A wave propagation study, based on vertical velocity distribution, showed that

lateral overhangs to some extent influence the average propagation velocity.

Furthermore, due to wave propagation, local failure mechanisms form at midspan, even before the effects of the impact load reach the supports. Therefore, beam length seems to play a minor role in the governing failure mechanism compared to the effective span length. This is especially critical for shear failure, as the effective shear slenderness is lower than the one corresponding to beam geometry. Consequently, it has been shown the relevance of knowing the evolution of inertia forces distribution and effective span when assessing beam strength under impact loading. Finally, it has also been proven different DIF for shear and bending strengths.

5. Acknowledgements

A substantial part of this work was carried out during a research stay of the corresponding author at Chalmers University of Technology. The financial support provided by the following sources is gratefully acknowledged: Swedish Civil Contingencies Agency, The Swedish Fortification Corp's Research Fund and Spanish Ministry of Economy (Project No. BIA2016-74960-R). In addition, the authors also thank "Fundación José Entrecanales Ibarra" for funding the PhD fellowship of the corresponding author. Also the authors would like to express their gratitude to Ph.D. Joosef Leppänen, Adj. Prof. Mathias Flansbjer and Sebastian Almfeldt at Chalmers University of Technology for kindly providing help with the experimental test used in this study.

6. References

[1] Kishi N, Mikami H, Matsuoka KG, Ando T. Impact behavior of shear-failure-type RC beams without shear rebar. *Int J Impact Eng* 2002; 27: 955–968.

[2] Micallef K, Sagaseta J, Fernández Ruiz M, Muttoni A. Assessing punching shear failure in reinforced concrete flat slabs subjected to localised impact loading. *Int J Impact Eng* 2014; 71: 17–33.

[3] Saatci S, Vecchio F. Effects of shear mechanisms on impact behavior of reinforced concrete beams. *ACI Struct J* 2009; 106: 78–86.

[4] Swedish Fortifications Agency. *Building Regulations FKR 2011. Dnr. 4535/2011 (In Swedish)*. Eskilstuna, Sweden, 2011.

[5] Swedish Civil Contingencies Agency. *Civil defence shelter SR 15 (In Swedish)*. Karlstad, Sweden, 2018.

[6] Ulzurrun GSD, Zanuy C. Enhancement of impact performance of reinforced concrete beams without stirrups by adding steel fibers. *Constr Build Mater* 2017; 145: 166–182.

[7] Isaac P, Darby A, Ibell T, Evernden M. Experimental investigation into the force propagation velocity due to hard impacts on reinforced concrete members. *Int J Impact Eng* 2017; 100: 131–138.

[8] Cotsovos DM, Stathopoulos ND, Zeris CA. Behavior of RC Beams Subjected to High Rates of Concentrated Loading. *J Struct Eng* 2008; 134: 1839–1851.

[9] Zhao D, Yi W, Kunnath SK. Shear Mechanisms in Reinforced Concrete Beams under Impact Loading. *J Sruct Eng* 2017; 143: 1–13.

[10] Dong YL, Pan B. A Review of Speckle Pattern Fabrication and Assessment for Digital Image Correlation. *Exp Mech* 2017; 57: 1161–1181.

[11] Kirugulige MS, Tippur H V., Denney TS. Measurement of transient deformations using digital image correlation method and high-speed photography: application to dynamic fracture. *Appl Opt* 2007; 46: 5083–5096.

[12] Jönsson J, Stenseke A. *Concrete Beams Subjected to Repeated Drop-Weight Impact and Static Load*. Chalmers TH, 2018.

[13] Johansson M, Rempling R, Ulzurrun GSD, Zanuy C. Key aspects of digital image correlation in impact tests of reinforced concrete beams. In: *Proceedings of the IABSE Symposium*. Guimarães, 2019.

[14] European Commitiee for Standardization. *EN 1992: Eurocode 2: Design of concrete structures*. Brussels, Belgium, 2004.

[15] Ulzurrun G, Zanuy C. Flexural response of SFRC under impact loading. *Constr Build Mater* 2017; 134: 397–411.

[16] McGhie RD. Flexural Wave Motion in Infinite Beam. *J Eng Mech* 1990; 116: 531–548.